Journal of The Electrochemical Society, 2026 **173** 064505

Towards Seawater Electrolysis in Alkaline Media: Assessing the Role of Hypochlorite Formation

Renaud Delmelle, Nathan Wauthy, Ronny Santoro, and Joris Proost[z]

Division of Materials and Process Engineering, Université catholique de Louvain (UCLouvain), Louvain-la-Neuve, Belgium

The chlorine ion present in seawater is the most threatening danger to water splitting technologies aiming at directly using the seawater as an electrolyte. In the alkaline route, chlorine can potentially be oxidized to hypochlorite, a toxic and corrosive compound that remains in the electrolyte in aqueous form. However, there is an electrochemical window allowing to completely avoid the formation of hypochlorite. In this work, a set of commercial electrodes and gas separators were tested in a lab-scale electrochemical cell by injecting different concentrations of Cl^- in the electrolyte and testing various operating conditions. The latter include varying the imposed current density and KOH concentration in the electrolyte at 70 °C. Our results show that the key parameter is the cell voltage, which, if kept under 1.9 V, enables to avoid ClO^- formation and its consequences, e.g. corrosion of the electrodes and bipolar plates. With our setup, this condition was successfully met by simultaneously using an electrolyte with at least 30 wt% KOH and limiting the current density to 0.5 A cm^{-2}.

 [DOI: 10.1149/1945-7111/ae4ffb]

Manuscript submitted December 15, 2025; revised manuscript received February 12, 2026. Published March 20, 2026.

As the global demand for clean energy intensifies, hydrogen has emerged as a pivotal solution for decarbonizing industrial processes, transportation, and power generation.[1,2] Water electrolysis, i.e. splitting water into hydrogen and oxygen using electricity, is a promising method for producing clean hydrogen, especially when powered by renewable energy sources.[3,4] While traditional electrolysis relies on purified freshwater, growing interest is shifting toward the use of seawater,[5] which constitutes over 96% of the Earth's water supply. Seawater electrolysis holds the promise of sustainable, large-scale hydrogen production without placing pressure on scarce freshwater resources.[6] At the same time, while seawater is abundant and freely available, the energy and materials cost required to maintain efficiency and durability can be significant.[7] in particular, the cost of corrosion-resistant materials and increased system maintenance must be offset by gains in scalability and environmental impact. Life-cycle assessments (LCAs) and techno-economic analyses suggest that while seawater electrolysis may not yet be economically superior to freshwater-based systems, it offers clear benefits in regions facing water scarcity,[8] and its potential improves significantly when coupled with offshore wind farms.[9]

Electrolysis of water involves the cathodic hydrogen evolution reaction (HER) and the anodic oxygen evolution reaction (OER). In seawater electrolysis, the complexity increases due to the presence of chloride (Cl^-).[10] These anions can compete with or interfere in the OER, leading to chlorine evolution reactions (CER) that not only reduce the faradaic efficiency of the anodic reaction but can also produce hazardous and toxic byproducts like chlorine gas (Cl_2) and hypochlorite (ClO^-) in acidic and alkaline media, respectively.[11] Moreover, for the latter, depending on the competitive interaction between OH^- and Cl^- at Ni surfaces, chloride-induced destabilization of $Ni(OH)_2$/NiOOH layers and Ni–Cl complexation can occur well before hypochlorite formation as well.[12–14] Finally, seawater's variable composition, affected by geographical and seasonal factors as illustrated in Table I,[15] adds further complexity to process optimization. For instance, the formation of insoluble metal hydroxides of divalent cations, in particular $Mg(OH)_2$ and $Ca(OH)_2$, can degrade electrode materials and obstruct ion transport.[6,16]

One obvious solution to avoid any issues related to chloride oxidation is to pre-treat the seawater by well-established techniques like reverse osmosis,[17] and only use the Cl^- free fraction for water electrolysis. However, this not only increases the spatial and energetic footprint, which becomes especially critical for off-shore hydrogen production, but also puts additional ecological constraints because of the need for a downstream brine treatment.[18] Therefore, efforts to develop direct seawater electrolysis systems that avoid pre-treatment are increasing. During such direct seawater electrolysis, the electrochemical reactions must be selectively tuned to favor water splitting over chloride oxidation. Many of them have concentrated so far on direct seawater electrolysis in acidic media, by adapting a classical Proton Exchange Membrane (PEM) electrolyser.[6,7,19] In this case, selective electrocatalysts that suppress the CER while promoting the OER are being developed. In particular, transition metal-based catalysts, such as nickel-iron (NiFe) layered double hydroxides (LDH), have already shown promising selectivity and stability.[20] Other studies have explored coating strategies, such as using hydrophobic or ion-selective membranes, to physically block Cl^- transport to the anode surface.[7,21]

PEM seawater electrolysis is often seen as a more promising technology than its alkaline counterpart, mostly because of its compactness.[6,22] This is mainly related to the common belief that alkaline electrolysers have a significantly higher footprint as compared to PEM: 100 m^2 MW^{-1} vs 50 m^2 MW^{-1}.[23] As a result, they are usually considered to be much less attractive for off-shore applications, despite their intrinsic higher durability, higher compatibility with seawater impurities and lower cost. However, this footprint-related argument needs to be revised with the emergence of high current density alkaline water electrolysis, both using a standard Zirfon diaphragm[24] or anion-exchange membranes (AEM);[25] but also following alternative approaches like in the case of capillary-fed electrolysis.[26]

In the Pourbaix diagram in Fig. 1, thermodynamically stable phases of the chlorine-water system in standard conditions are shown, with solid black lines representing the equilibrium conditions between two regions where different species are predominant. The region between the two dashed red lines represent the stability region of water, and the regions above and below that region represent the stability regions of oxygen and hydrogen, respectively. From this diagram, it becomes clear that, in alkaline media, the challenge of favoring water splitting over chloride oxidation becomes somewhat relaxed. First of all, for pH $>$ 7, the stable species resulting from chloride oxidation is no longer chlorine gas, but aqueous hypochlorite ClO^-:

$$Cl^- + 2OH^- = ClO^- + H_2O + 2e^- \quad [1]$$

Kinetically, this 2 electron exchange reaction involves a 2-step Volmer-Heyrovsky mechanism:

[z]E-mail: joris.proost@uclouvain.be

Table I. Most prevalent ions in seawater and their concentration in mmol/L at different locations.

mmol/l	Na^+	Mg^{2+}	Ca^{2+}	K^+	Cl^-	SO_4^{2-}
"Standard" seawater	469	52.7	10.3	10.2	553	28.2
Atlantic ocean	493	55.1	10.8	10.9	577	29.5
North sea	478	54.6	11.9	10.3	569	28.4
Baltic sea	99	10.5	2.6	2.2	116	6.0
Mediterranean sea	515	62.3	10	9.5	615	22.4

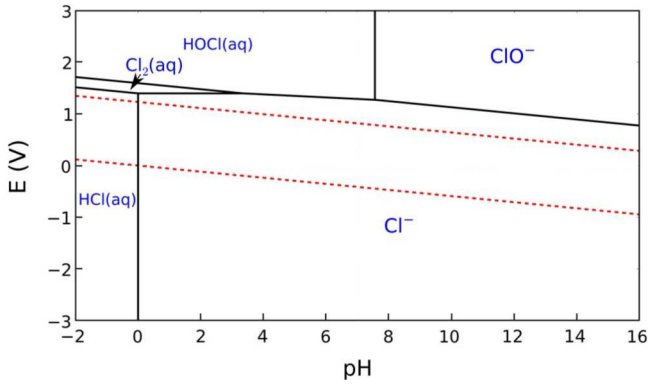

Figure 1. Pourbaix diagram of the chlorine-water system at 25 °C. Reproduced from Ref. 27.

Volmer step:

$$M + Cl^- = M - Cl + e^- \quad [2]$$

Heyrovsky step:

$$M - Cl + 2OH^- = M + ClO^- + H_2O + e^- \quad [3]$$

with M representing an electrocatalytically active site on the surface of the anode, either metallic or oxidized.[28]

Secondly, at pH > 7, the electrochemical window that allows to avoid ClO^- formation (~480 mV, cfr. Figure 1) is significantly larger than the one to avoid Cl_2 formation (~100 mV at pH ⩽ 0). On the other hand, contrary to gaseous Cl_2 which can be captured or vented to the atmosphere, aqueous hypochlorite ions remain in solution. As such, they present a strongly oxidising agent that is not only highly corrosive to the metal electrodes and piping,[21] but is also toxic to marine life and human health.[29] Moreover, hypochlorite ions can undergo further oxidation to chlorite (ClO_2^-), chlorate (ClO_3^-) and perchlorate (ClO_4^-), thereby further decreasing the anodic Faradaic efficiency of the water oxidation reaction itself.[7,21]

The objective of the current work is to demonstrate that, under certain conditions, direct seawater electrolyis in alkaline media is feasible without any hypochlorite formation, using the same Ni-based electrodes, diaphragm and KOH electrolyte concentration as in state-of-the-art alkaline water electrolysers. At the same time, we also demonstrated that, if hypochlorite formation is not suppressed, all cell components, including electrodes, diaphragm and cell housing, are severely corroded within one hour of operation.

Experimental

Electrochemical characterisation.—For the water electrolysis experiments, we used the same home-built flow-through cell already described in previous work,[30] and represented in Fig. 2. For the electrodes, 0.5 mm thick expanded Ni meshes were used, coated with Pt or RuO_2 on the anode and cathode side, respectively. They were obtained directly from the industrial alkaline electrolyser manufacturer Hydrogenics who had it in stock for their 300 cm^2 prototype stack, and then cut to 2 × 2 cm^2 square electrodes to fit into our own electrochemical cell. Although the exact structural details and coating procedures of these expanded Ni meshes cannot be disclosed, a view on their surfaces can be taken on the Scanning Electron Microscopy (SEM) images in Fig. 3, acquired with a Zeiss Ultra 55 microscope operating at 15 kV. The expanded meshes of the cathode and anode from Figs. 3a and 3c have different structures, and their surfaces also show distinct profiles. The zoom of the cathode surface in Fig. 3b reveals bright flakes standing on a darker surface, the flakes likely showing electrical charging from ruthenium oxide. A closer look on the anode in Fig. 3d shows a more homogeneous, slightly cracked surface. A more detailed characterization study of these electrodes, including Energy Dispersive X-ray spectroscopy (EDX) quantification and X-ray Diffraction (XRD) analyses, is available in Ref. 31. Rather than using a knitted mesh to contact the electrodes to the Ni current collector plates, we used a 3000 μm pore sized, 4 mm thick Ni foam. Previous work demonstrated this to provide more reproducible data when compressing the cell during assembly. Cathodic and anodic compartments were separated by a commercial 500 μm thick Zirfon UTP 500 diaphragm (Agfa). All electrochemical experiments were carried out at 70 °C, a temperature which was controlled by 2 independent thermocouples immersed into separate stainless steel catholyte and anolyte reservoirs that were placed on a heating plate. Electrochemical data were collected using an AMETEK VersaSTAT3–200 potentiostat. Both cyclic-voltammetry (CV) and galvanostatic experiments were performed. For the first, the current density was cycled back and forth between 0 and 0.5 A cm^{-2} for 6 consecutive cycles at a scan rate of 0.01 A s^{-1}. Then, 5 min galvanostatic steps were included at 0.125, 0.25, 0.375 and 0.5 A cm^{-2}, respectively, in order to verify any possible electrochemical differences between dynamic and static loading. After that, 6 more CV cycles were imposed. Apart from these CV cycles, 6 h galvanostatic experiments at 0.5 A cm^{-2} have been performed as well to have an initial assessment of the longer-term stability.

For the electrolyte, both 1.0 M and 30 wt% KOH (>85%, VWR, NORMAPUR) solutions have been considered. While the latter, corresponding to about 6.9 M KOH, is the standard concentration for industrial alkaline electrolysers operating with a Zirfon diaphragm, a less concentrated 1.0 M solution is typically used for anion exchange membrane (AEM) alkaline electrolysis. Moreover, decreasing the KOH concentration also allows to test the effect of a less corrosive KOH medium. To both electrolytes, different concentrations of KCl were added (0.1, 0.5 and 1.0 M, > 99.5%, Merck Millipore, EMSURE) to both the catholyte and anolyte in order to simulate the effect of chlorine anions Cl^- present in seawater. For this work, we preferred to add the chloride as KCl, rather than as NaCl which is typically present in seawaters. This allowed to concentrate on the single effect of Cl^- addition, K^+ already being present in excess from the KOH electrolyte. It should be noted though that by doing so, possible synergistic effect that other anions might have, in particular sulfate (SO_4^{2-}, cfr. Table I) are overlooked. The latter has indeed been reported to help suppressing the CER through its preferential adsorption on the anode surface, forming a negative charge layer repelling the chloride ions through electrostatic repulsion.[32]

In our set-up, catholyte and anolyte were never mixed, but pumped through the cell via 2 separate peristaltic pumps (Cole-Parmer, Model 7553–77) at a moderate flow rate of 0.9 L min^{-1}. Both the catholyte and anolyte reservoirs were connected to a separate transparent gas collection reservoir. These were used to have an independent measurement of the Faradaic efficiency by observing the gas volume evolution over time during a galvanostatic experiment (at 2 A) performed separate from the CV and galvanostatic experiments described above. Finally, the electrical conductivity of the electrolytes considered in this study was measured ex situ using a 914 pH/Conductometer instrument from Metrohm.

Hypochlorite and metallic ions characterisation.—While the presence of Cl^- may lead to chlorine gas (Cl_2) formation during

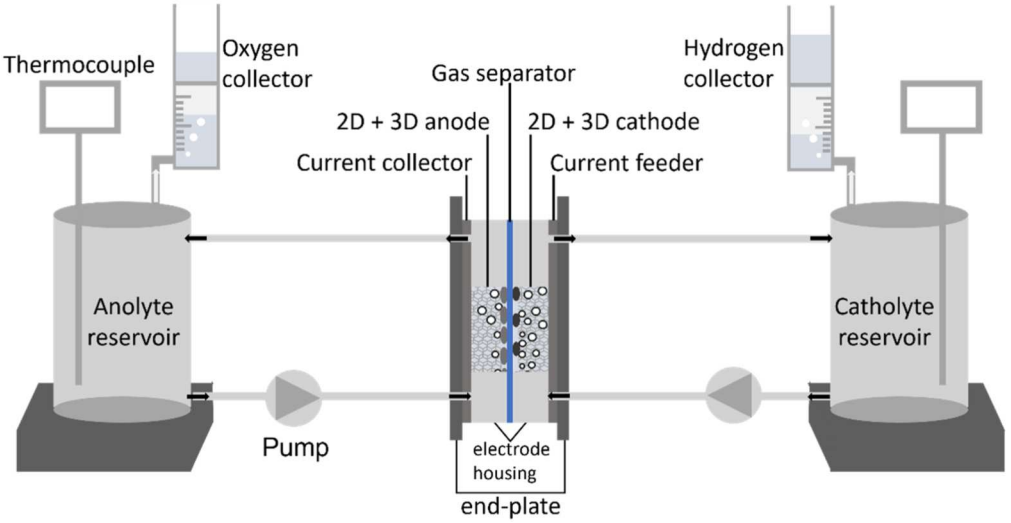

Figure 2. Schematic representation of the experimental setup used in the present study.

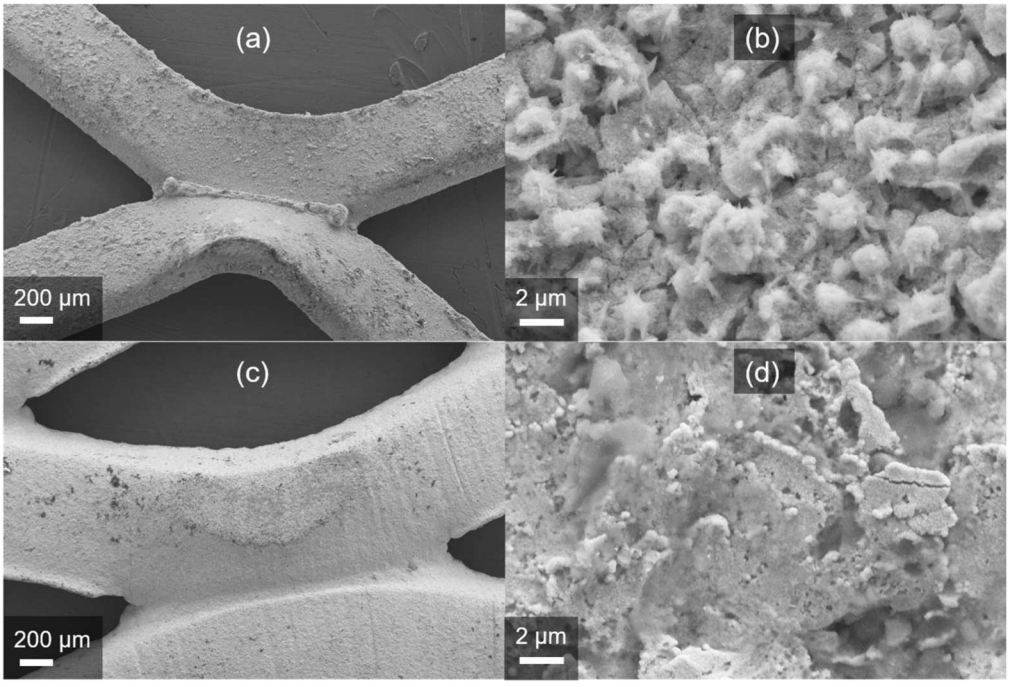

Figure 3. SEM images of the structures of the expanded meshes of the cathode (a) and anode (c) used in this study, together with zooms on the corresponding cathode (b) and anode (d) surfaces.

water oxidation in acid media, oxidation of Cl^- into aqueous hypochlorite (ClO^-) is be expected for pH $>$ 7 (cfr. Figure 1). Its detection is not straightforward, and requires a dedicated analytical protocol.[33] The o-tolidine method consists in reacting the hypochlorite with o-tolidine and measuring the absorbance of the resulting solution. Selected concentrations of ClO^- were added to our KOH solutions (15 µM, 30 µM, 45 µM, 60 µM and 90 µM for the 1 M KOH solution and 15 µM, 30 µM, 45 µM, 60 µM, 105 µM, 150 µM, 195 µM, 285 µM, 390 µM, 495 µM, 600 µM and 690 µM for the 30 wt% KOH solution, 0.1 ml each), which in turn were added to a test solution of 0.5 mM o-tolidine in order to obtain a calibration curve. The UV–vis spectra were then measured (with a SPECORD 200 plus from Analytik Jena) at a wavelength of 436 nm in order to extract the evolution of the absorbance as a function of the hypochlorite concentration.

Resulting calibration curves for the 2 electrolytes considered in this work are shown in Fig. 4. In order to eliminate any analytical interference with other impurities known to occur during alkaline water electrolysis (in particular dissolved Fe^{2+} when using a stainless steel set-up[34]), long-term (6 hr) galvanostatic experiments were repeated in a full glass setup, during which the anolyte was sampled every hour for an ex situ hypochlorite characterization, as well as inductively coupled plasma—optical emission spectrometry (ICP-OES, model Varian 720-ES) for detection of metallic elements.

Results and Discussion

As a starting point for the electrochemical analysis, Fig. 5 shows the effect of different Cl^- concentrations on the polarisation curves for alkaline water electrolysis using two KOH concentrations: 30 wt % KOH on the left, and 1.0 M KOH on the right, respectively.

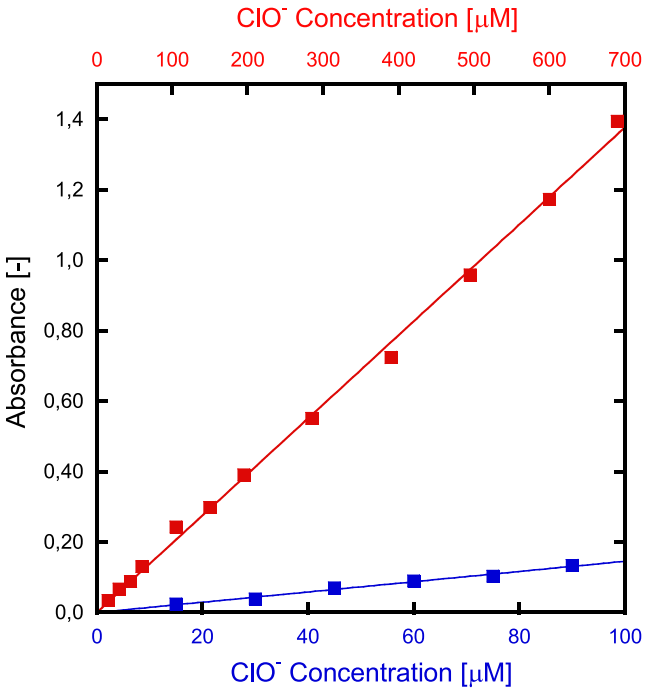

Figure 4. ClO^- calibration curves corresponding to the two electrolyte solutions used in this study (blue: 30 wt% KOH, red: 1 M KOH), obtained by measuring the absorbance of these solutions after adding o-tolidine.

Superposed on the last recorded CV-curve for each condition are the average cell voltages obtained during the 5 min galvanostatic stays at 0.125, 0.25, 0.375 and 0.5 A cm^{-2} that were performed in-between the 2×6 CV cycles. The fact that in both cases no difference is observed indicates that the dynamic (CV) and static (galvanostatic) behaviour is identical. When comparing the effect of the Cl^- additions for the two KOH concentrations, no effect could be observed in 30 wt% KOH (Fig. 5a, left), while a decreasing trend with increasing Cl^- is evident in 1.0 M KOH (Fig. 5b, right). Before considering unwanted reactions involving chloride, the cell voltage is likely affected by the increase in electrical conductivity of the electrolyte induced by the addition of KCl, especially in the 1.0 M KOH electrolyte. Indeed, the conductivity of electrolyte specimens was measured ex situ at 70 °C, revealing a 26% increase in conductivity after the addition of 1.0 M KCl to the 1.0 M KOH electrolyte, while the 30 wt% KOH electrolyte did not undergo any sensible change in conductivity after adding the same amount of KCl.

Since the polarisation curves shown in Fig. 5 cover a relatively broad cell voltage range, starting already from about 1.4 V at near-zero current density, oxidation reactions occurring at low potentials that affect the Ni electrode chemistry might explain part of the differences observed. A particularly useful literature report is Ref. 32, which explored the effect of ion concentrations on the electrode activity and stability during direct alkaline seawater electrolysis. In that study, it was shown how in NaOH-based electrolytes at low current densities (10 mA cm^{-2}, corresponding in that study to an overpotential of 300–400 mV), the mass of $Ni(OH)_2$ on Ni foam anodes in the absence of Cl^- was decreased 2-fold when going from 1.0 M to 6.0 M NaOH. At the same time, increasing the Cl^- concentration by adding up to 1.8 M NaCl at the same low current density to a 6.0 M NaOH electrolyte solution increased the mass of $Ni(OH)_2$ almost 4-fold, without any sign of Cl^- consumption. Therefore, in the low potential range of the polarisation curves shown in Fig. 5, we cannot rule out the dominant role of Ni-Cl interactions in tuning the Ni anode chemistry, rather than initiating hypochlorite formation. The following reaction steps that underly such Ni-Cl interactions and at the same time affect $Ni(OH)_2$ formation have been proposed in Ref. 32 as follows:

$$Ni + Cl^- = NiCl_{ads} + e^- \quad [4]$$

$$NiCl_{ads} + Cl^- = NiCl_x^- \quad [5]$$

$$NiCl_x^- + OH^- = Ni(OH)_2 + Cl^- \quad [6]$$

In addition to the polarisation curves of Fig. 5, measurements of the Faradaic efficiency for each Cl^- concentration were performed during dedicated galvanostatic stays at 0.5 A cm^{-2}, which is the highest current density. Results are shown in Fig. 6, both for the anodic (O_2 evolution) and cathodic (H_2 evolution) compartment. For the 30 wt% KOH electrolyte, no effect of Cl^- could be detected, with Faradaic efficiencies for both the O_2 and H_2 evolution reaction being statistically equal to 100%. For the 1.0 M KOH electrolyte, a significant decrease in the anodic Faradaic efficiency was observed, with values decreasing to about 80% and 30% for Cl^- concentrations of 0.5 M and 1.0 M, respectively. At the same time, similarly as for the 30 wt% KOH condition, cathodic Faradaic efficiencies related to the H_2 evolution reaction remained at 100%, independent of Cl^- concentration.

One possibility for the decrease in anodic Faradaic efficiency with increasing Cl^- concentration in the 1.0 M KOH electrolyte under such high potential conditions is the gradual oxidation of chloride Cl^- to hypochlorite ClO^-. According to the Pourbaix

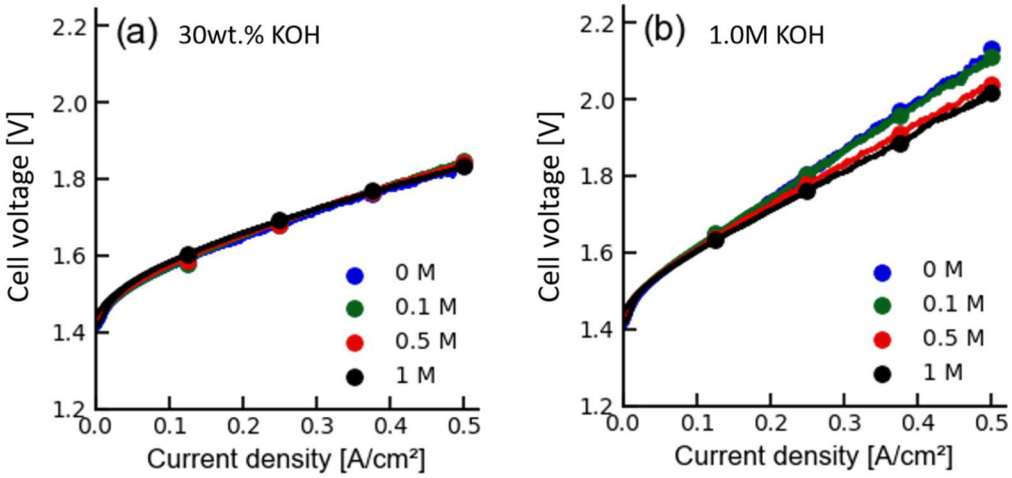

Figure 5. Polarisation curves at 70 °C, (a) 30 wt% KOH and (b) 1 M KOH, for 4 different concentrations of KCl added to the electrolyte. Separator: Zirfon diaphragm. Electrodes: coated, expanded Ni meshes combined with a 3000 μm pore sized Ni foam. Lines are measured from cyclic voltammetry, with superimposed bullet points from 5 min galvanostatic experiments.

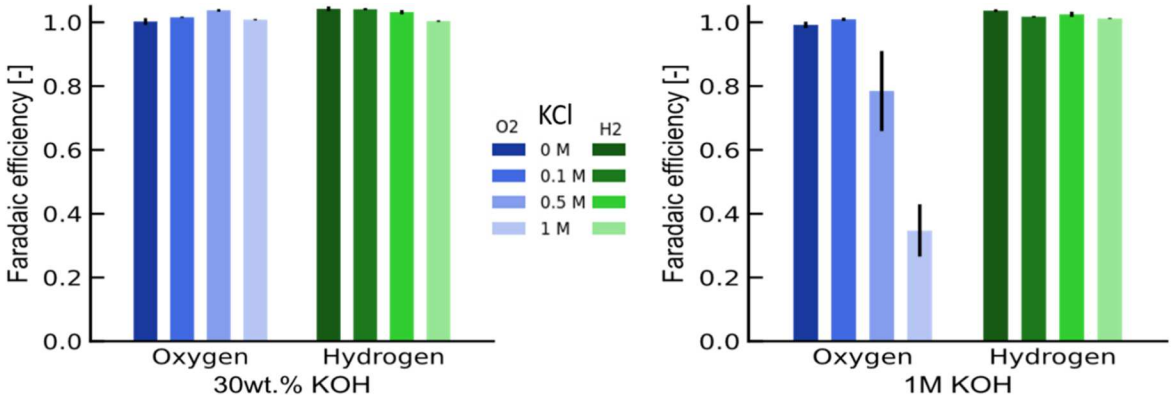

Figure 6. Faradaic efficiency, presented as bar charts, both on the oxygen and hydrogen sides, in 1 M KOH and 30 wt% KOH, and for 4 different concentrations of KCl added to the electrolyte. Efficiencies are measured during galvanostatic steps at 70 °C and 0.5 A cm^{-2}.

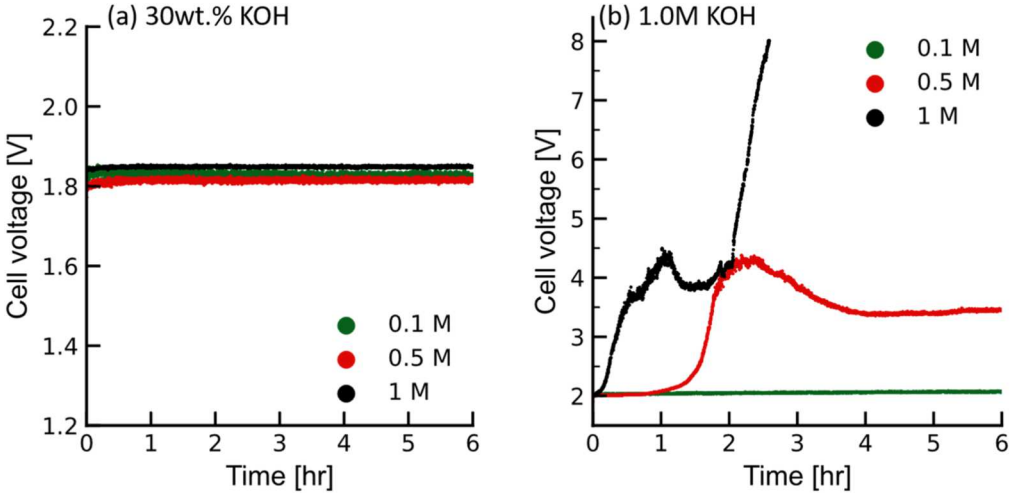

Figure 7. Cell voltage evolution during a 6 h galvanostatic experiment at 0.5 A cm^{-2}, 70 °C, for (a) 30 wt% KOH and (b) 1 M KOH electrolyte solutions, for 3 different concentrations of KCl added to the electrolyte.

diagram already shown in Fig. 1, such an oxidation can be expected to occur simultaneously with the water oxidation reaction for cell voltages exceeding 1.9 V. Indeed, the voltage difference between the standard equilibrium lines for water dissociation on the Pourbaix diagram is 1.23 V (red dotted lines in Fig. 1). When adding at pH > 7 an overpotential of 480 mV, which is a typical value encountered for the OER during alkaline water electrolysis,[35] one already passes above the equilibrium line for Cl^- oxidation, thereby hitting the ClO^- stability region. Since for the HER a minimum overpotential of 0.19 V is usually required as well,[36] any cell voltage above 1.23 + 0.48 + 0.19 = 1.9 V would cause the simultaneous oxidation of both water into O_2 and Cl^- into ClO^-. Since hypochlorite is an aqueous species dissolved in the electrolyte, contrary to the gaseous OER, its formation will not contribute to the measured gas volume on which the anodic Faradaic efficiency values are based. This then explains their significant decrease observed in Fig. 6b on the anodic side.

We acknowledge that, since our electrochemical flow-through cell set-up does not allow for separate anodic and cathodic half-cell potential measurements, the above thermodynamic argument relating hypchlorite formation to the total cell voltage remains speculative. Therefore, in order to confirm the hypothesis of hypochlorite formation once the cell voltage exceeds 1.9 V, additional long-term (6 hr) galvanostatic experiments were performed at 0.5 A cm^{-2} for different Cl^- concentrations. During these experiments, anolyte samples were taken every hour, and analysed quantitatively for their ClO^- concentration, as well as their concentrations of metallic species potentially coming from the stainless steel elements of the setup (Fe, Cr, Mo) and from the electrodes (Ni). Figure 7 shows the corresponding cell voltage evolution, both for the 30 wt% KOH and the 1.0 M KOH electrolyte. For the 30 wt% KOH electrolyte (Fig. 7a, left), no significant differences could be observed for the different Cl^- concentrations, as was also the case for the polarisation curves reported in Fig. 5a. Moreover, the cell voltage remains very stable over time as well. This suggests that even in the presence of up to 1.0 M Cl^- (which is twice the typical concentration of Cl^- in seawater), no degradation of the cell components has occurred. On the contrary, for the 1.0 M KOH electrolyte (Fig. 7b, right), a significant degradation can be expected in the presence of 0.5 and 1.0 M of Cl^- from the observed cell voltage increase up to 4 and 8 V, respectively. As seen in Fig. 8, in the case of 0.5 M Cl^-, this voltage increase can be correlated to a significant increase in ClO^- concentration detected in the 1.0 M KOH anolyte. At the same time, no sign of hypochlorite formation could be detected in the 30 wt% KOH anolyte, its concentration always remaining under the detection limit of our analytical protocol. We do need to acknowledge though that, besides the thermodynamic argument related to the lower cell voltage in the case of 30 wt% KOH, the competitive interaction between OH^- and Cl^- at the surface of our Ni-based electrodes, as described by reactions (3) and (4), is also in favor of OH^- adsorption at higher KOH concentrations. This kinetic argument may therefore have contributed as well to favoring O_2 evolution over hypochlorite formation in the case of 30 wt% KOH.

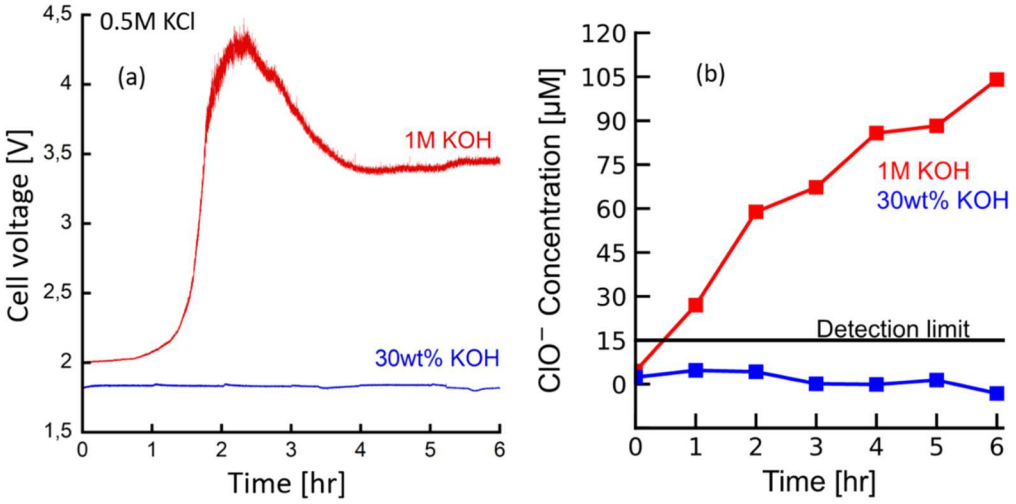

Figure 8. (a) Cell voltage evolution during a 6-hours galvanostatic experiment at 0.5 A cm^{-2}, 0.5 M KCl, 70 °C, for 1 M KOH (red) and 30 wt% KOH (blue) electrolyte solutions; and (b) corresponding ClO^- concentrations in the electrolyte measured by the o-tolidine method in a full-glass setup.

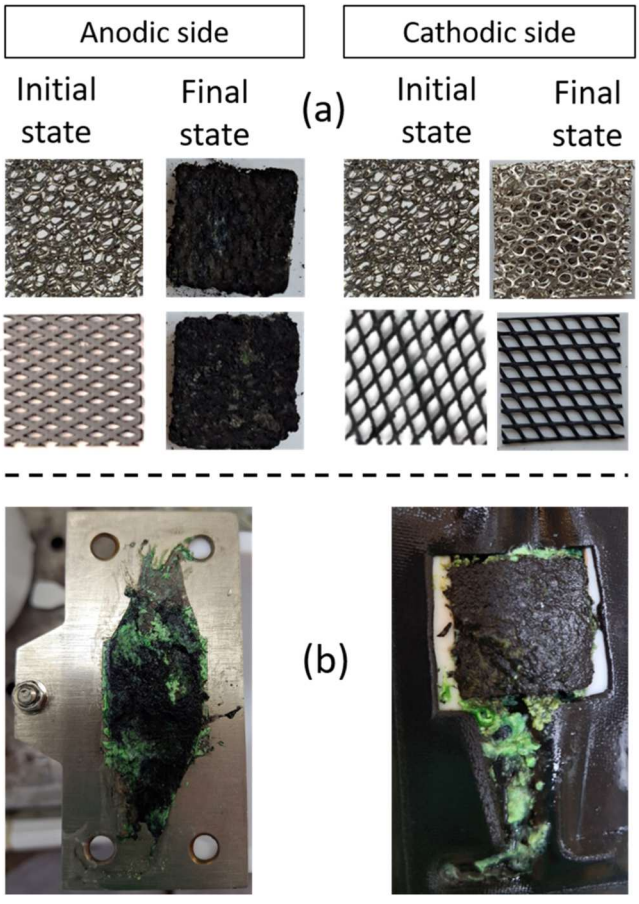

Figure 9. Photographs of (a) the 2 × 2 cm^2 anodes and cathodes before and after a 6 h galvanostatic test at 0.5 A cm^{-2} and 70 °C in a 1 M KOH + 0.5 M KCl electrolyte, showing the Ni foams on top and the Ni expanded meshes on the bottom and (b) the anodic bipolar plate (left) and the cathode and its sealing (right) after a 6 h galvanostatic test performed at 0.5 A cm^{-2} and 70 °C in a 1 M KOH + 1 M KCl electrolyte.

Anolyte samples taken during the experiments performed in the stainless steel setup revealed, after ICP analysis, accumulation of metallic ions in the electrolyte, especially Fe^{2+} (17.6 mg l^{-1} after 6 h) and Cr^{2+} (9.6 mg l^{-1} after 6 h). These elements significantly modified the absorbance of the liquid samples, in turn perturbing the hypochlorite characterisation. Therefore, the galvanostatic steps of Fig. 8a were repeated in a full glass setup in order to obtain the correct ClO^- concentration values, shown in Fig. 8b. In the latter setup, all metallic elements measured by ICP remained under 0.2 mg l^{-1}, and did not show any signs of accumulation.

Finally, Fig. 9 allows to visually anticipate the effect of hypochlorite formation on the dramatic cell voltage increase in the 1.0 M KOH electrolyte. It shows on the one hand (Fig. 9a, left) optical micrographs of anode degradation after 6 hr exposure to 0.5 M Cl^-, both the catalytically coated perforated Ni plate and the 3000 µm Ni foam used as porous transport layer. Even more dramatically, Fig. 9b shows pictures of the entire flow-through cell after 6 hr exposure to 1.0 M Cl^-. For the latter, not only the anodes show significant traces of ClO^- induced corrosion, but also the Ni current collector plate has started to corrode. This is not surprising, since ClO^- is well-known to be a strongly corroding agent, sometimes even called "bleach".[29]

Conclusions

This study assessed the role of hypochlorite formation on the performance and integrity of alkaline seawater electrolysers. While the concentration of Cl^- in the seawater is an important starting parameter for its progressive oxidation to ClO^-, we have shown that depending on the electrolyser operating conditions, hypochlorite formation can be completely avoided. In particular, it was shown that when operating a seawater electrolyser with both an alkaline anolyte and catholyte that contains Cl^- concentrations exceeding 0.5 M, its electrochemical window should guarantee that the cell voltage remains below 1.9 V. In this work, we have demonstrated that this can be done by using a KOH electrolyte that is sufficiently concentrated (at least 30 wt% KOH) while at the same time limiting the current density to 0.5 A cm^{-2}.

Acknowledgments

Funding from the Belgian Energy Transition Funds (ETF) of the Federal Planning Service for Economy, S.M.E., Self-employment and Energy is gratefully acknowledged through the MuSE project (Molecules at Sea).

ORCID

Renaud Delmelle https://orcid.org/0000-0003-1455-4656
Nathan Wauthy https://orcid.org/0009-0005-8497-9969
Ronny Santoro https://orcid.org/0009-0007-3204-9940
Joris Proost https://orcid.org/0000-0003-2220-1893

References

1. J. Jacquemin, P. Thiran, and S. Quoilin, "Prioritizing the role of renewable fuels and hydrogen networks in the transition towards net zero emissions in Western Europe." *Energy*, **314**, 134069 (2025).
2. S. Evro, B. A. Oni, and O. S. Tomowedo, "Carbon neutrality and hydrogen energy systems." *Int. J. Hydrogen Energy*, **78**, 1449 (2024).
3. J. Brauns and T. Turek, "Experimental evaluation of dynamic operating concepts for alkaline water electrolyzers powered by renewable energy." *Electrochim. Acta*, **404**, 139715 (2022).
4. N. A. Burton, R. V. Padilla, A. Rose, and H. Habibullah, "Increasing the efficiency of hydrogen production from solar powered water electrolysis." *Renew. Sustain. Energy Rev.*, **135**, 110255 (2021).
5. Z. Guan, Y. Zhong, L. Kong, B. Chen, W. Li, Z. Shi, R. Zhang, J. Wu, and Z. Fu, "Research progress and prospects of electrocatalytic seawater electrolysis for hydrogen production." *J. Electroanal. Chem.*, **1000**, 119638 (2026).
6. S. Mahadik et al., "Seawater electrolysis: Unlocking a new path for hydrogen production." *EnergyChem*, **7**, 100173 (2025).
7. S. Khatun, H. Hirani, and P. Roy, "Seawater electrolysis: Aactivity and selectivity." *J. Mater. Chem. A*, **9**, 74 (2021).
8. R. Kumar, A. Sharma, P. Kumar, K. S. Kiran, H. M. Albert, A. P. Agrawal, G. Raj. R., B. Challa, G. V. Rambadu, and A. Kumar, "Advanced materials and system innovations for seawater electrolysis in hybrid renewable energy systems: Toward sustainable hydrogen production." *Chem. Phys. Impact*, **11**, 100972 (2025).
9. M. Mehrpooya, P. A. Dezfouli, and M. Shafiee, "Integrated techno-economic modelling and analysis of a wind-powered seawater reverse osmosis desalination plant with hydrogen storage as a backup system." *Int. J. Hydrogen Energy*, **186**, 152031 (2025).
10. , S. Ghosh, T. K. Fathima, and S. Ramaprabhu, "Rational design of bifunctional catalysts for chlorine-free, durable overall seawater electrolysis." *Electrochim. Acta*, **503**, 144803 (2024).
11. N. Raza, "Challenges and solutions in suppressing chlorine evolution reaction in seawater electrolysis." *J. Power Sources*, **659**, 238331 (2025).
12. A. Gaur, E. Enkhbayar, J. Sharma, S. Mhin, and H. Han, "Chloride-ion blocking in seawater electrolysis: narrating the tale of likes and dislikes between anode and ions." *Energy Environ. Mater.*, **8**, e128170 (2025).
13. D. He, P. Yang, K. Yang, J. Qiu, and Z. Wang, "Durable seawater electrolysis enabled by chloride rejection on hydroxide trapping anode." *J. Energy Chem.*, **107**, 407 (2025).
14. L. R. Czarnetzki and L. J. J. Janssen, "Formation of hypochlorite, chlorate and oxygen during NaCl electrolysis from alkaline solutions at an RuO_2/TiO_2 anode." *J. Appl. Electrochem.*, **22**, 315 (1992).
15. P. Loganathan, G. Naidua, and S. Vigneswaran, "Mining valuable minerals from seawater: A critical review." *Environ. Sci. Water Res. Technol.*, **3**, 37 (2017).
16. H. Qazi, D. Chauhan, and Y.-H. Ahn, "Impurity impacts and mitigation strategies in alkaline seawater electrolysis." *Int. J. Hydrogen Energy*, **99**, 155 (2025).
17. K. Park, J. Kim, D. R. Yang, and S. Hong, "Towards a low-energy seawater reverse osmosis desalination plant: A review and theoretical analysis for future directions." *J. Membr. Sci.*, **595**, 117607 (2020).
18. A. Panagopoulos and K.-J. Haralambous, "Environmental impacts of desalination and brine treatment - challenges and mitigation measures." *Mar. Pollut. Bull.*, **161**, 111773 (2020).
19. J. Guo, Y. Zheng, Z. Hu, C. Zheng, J. Mao, K. Du, M. Jaroniec, S.-Z. Qiao, and T. Ling, "Direct seawater electrolysis by adjusting the local reaction environment of a catalyst." *Nat. Energy*, **8**, 264 (2023).
20. W. He et al., "Materials design and system innovation for direct and indirect seawater electrolysis." *ACS Nano*, **17**, 22227 (2023).
21. S. Li et al., "Mitigating chlorine-induced damage: Advances in chlorine corrosion mechanisms and anti-corrosion strategies for anode catalysts in hydrogen production via seawater electrolysis." *J. Energy Chem.*, **113**, 484 (2026).
22. B. Shetty, S. Puranam-Rajashekar, G. H. Aralikatti, P. Nagaraj, L. H. Kumar, P. N. Tengli, M. S. Thakur, Sridhar V, and M. Krishnappa, "Seawater electrolysis: A critical review on fundamentals, recent progress, and future perspectives on sustainable hydrogen generation." *Next Energy*, **9**, 100407 (2025).
23. International Energy Agency, *The Future of Hydrogen* (2019), https://iea.org/reports/the-future-of-hydrogen/.
24. F. Rocha et al., "Proton exchange membrane-like alkaline water electrolysis using flow-engineered three-dimensional electrodes." *Nat. Commun.*, **15**, 7444 (2024).
25. M. Medina, A. Brunca da Silva, L. Xia, W. Jiang, A. Glüsen, C. Ribeiro, and L. H. Mascaro, "Tailoring NiFeS microsctucture through electrodeposition for high-performance anion exchange membrane water electrolysis." *J. Power Sources*, **657**, 238128 (2025).
26. A. Hodges, A. L. Hoang, G. Tsekouras, K. Wagner, C.-Y. Lee, G. F. Swiegers, and G. G. Wallace, "A high-performance capillary-fed electrolysis cell promises cost-competitive renewable hydrogen." *Nat. Commun.*, **13**, 1304 (2022).
27. R. K. N. Karlsson and A. Cornell, "Selectivity between oxygen and chlorine evolution in the chlor-alkali and chlorate processes." *Chem. Rev.*, **116**, 2982 (2016).
28. X. Zhang, L. Tong, Q. Huang, X. Liang, X. Shi, X. Bai, C.-Z. Wang, Y. Liu, S. Lin, and X. Zou, "Substrate-adaptive sacrificial corrosion strategy enables 700mV oxygen evolution window for enhanced seawater electrolysis." *Nature Comm.*, **17**, 757 (2026).
29. W. Luttrell, "Toxic tips: sodium hypochlorite." *J. Chem. Health Saf.*, **8**, 24 (2001).
30. F. Rocha, R. Delmelle, C. Georgiadis, and J. Proost, "Effect of pore size and electrolyte flow rate on the bubble removal efficiency of 3D pure Ni foam electrodes during alkaline water electrolysis." *J. Environ. Chem. Eng.*, **10**, 107648 (2022).
31. B. Lelotte, *Électrodes 3D Structures Pour L'électrolyse Alkaline De L'eau: Une étude Comparative. Ecole Polytechnique De Louvain, Université Catholique De Louvain* (2020), Prom.: J. Proost http://hdl.handle.net/2078.1/thesis:25320.
32. T. He, Q. Liu, H. Fan, Y. Yang, H. Wang, S. Zhang, R. Che, and E. Wang, "Exploring the effect of ion concentrations on the electrode activity and stability for direct alkaline seawater electrolysis." *Int. J. Hydrogen Energy*, **48**, 19385 (2023).
33. H. Xie, Z. Zhao, T. Liu, Y. Wu, C. Lan, W. Jiang, L. Zhu, Y. Wang, D. Yang, and Z. Shao, "A membrane-based seawater electrolyser for hydrogen generation." *Nature*, **612**, 673 (2022).
34. M. T. de Groot, "Alkaline water electrolysis: With or without iron in the electrolyte?" *Curr. Opin. Chem. Eng.*, **42**, 100981 (2023).
35. M. Plevová, J. Hnát, and K. Bouzek, "Electrocatalysts for the oxygen evolution reaction in alkaline and neutral media." *J. Power Sources*, **507**, 230072 (2021).
36. Y. Shi et al., "Hydrogen evolution electrodes: Materials and mechanisms in alkaline electrolysis." *Desalination*, **586**, 117887 (2024).